Tunneling conductance for *d*-wave superconductors: Dependence on crystallographic orientation and Fermi surface

P. Pairor and M. B. Walker
Department of Physics, University of Toronto, Toronto, Ontario, Canada M5S 1A7
(Received 2 August 2001; published 15 January 2002)

The dependence of the ab-plane differential conductance of a normal-metal-insulator-$d_{a^2-b^2}$-wave superconductor junction on the superconductor crystal orientation and its Fermi surface is investigated using a two-dimensional square lattice model. In the tunneling limit, when the orientation is away from {100} and {110}, the study shows that there are features at other energies in addition to a zero-bias conductance peak and a shoulderlike feature at the maximum gap. These additional features are found to occur at either the energy gap of the state with the momentum normal to the surface or the gap of the state with the momentum on the edge of the surface-adapted Brillouin zone, or at both of the energy gaps, depending on the shape of the Fermi surface. These considerations show that, in principle, tunneling can be used to determine the energy gap at wave vectors other than those at which the gap is at a maximum.

DOI: 10.1103/PhysRevB.65.064507 PACS number(s): 74.20.−z, 74.25.Jb

I. INTRODUCTION

Normal-metal-insulator-superconductor (NIS) tunneling spectroscopy is one of the most powerful tools used to study the quasiparticle excitations of a superconductor.[1,2] It provided the demonstration of the Bardeen-Cooper-Shrieffer (BCS) prediction of the density of states (DOS) of conventional *s*-wave superconductors as well as the measurement of their superconducting gaps.[3] The tunneling conductance of an isotropic *s*-wave superconductor is approximately proportional to its bulk DOS and does not depend on the crystallographic orientation of the superconductor.

In the past decade the technique of tunneling spectroscopy has been applied to the study of the quasiparticle excitations in high-T_c cuprates. The tunneling conductance spectra of these materials show strong dependence on the superconductor crystallographic orientation,[4–6] which is as expected for superconductors with an anisotropic gap function. The tunneling conductances of these superconductors do not always reflect the bulk DOS; instead they are closely related to the local DOS which strongly depends on the surface orientation.[7] Particularly in a *d*-wave superconductor, because zero-energy surface bound states[8] can be formed for certain surface orientations due to the change of sign of the gap function, the tunneling conductance curves can contain a peak at zero energy. Zero-bias conductance peaks (ZBCP's) have in fact been observed in many ab-plane tunneling experiments of cuprate superconductors.[4,9–15] The existence of the ZBCP is one of the strong pieces of evidence suggesting that the pairing symmetry of high-T_c cuprate superconductors is predominantly *d* wave.[8,16]

Quantitatively, one can understand the dependence on the surface orientation of the tunneling conductance of a *d*-wave superconductor by using a simple method, the so-called Blonder-Tinkham-Klapwijk (BTK) formalism.[17] This formalism makes use of the Bogoliubov–de Gennes (BdG) equation and the scattering method, which was first introduced to the study of the normal-metal-superconductor interface by Demers and Griffin.[18,19] Tanaka and Kashiwaya[20] make use of the formalism, together with a simple assumption that the Fermi surface of a $d_{a^2-b^2}$-wave superconductor is isotropic, to explain the evolution with the surface orientation of the ZBCP in the ab-plane tunneling conductance spectrum. They found that for {100} surfaces there is no ZBCP, and for surface orientations away from {100}, the ZBCP starts to appear. It reaches the biggest width and height when the surface orientation is {110}.

In addition to the ZBCP, a cusplike feature in the tunneling conductance spectrum also evolves with the surface orientation. It occurs at the maximum gap for {100} surfaces and disappears for {110} surfaces (there appears a shoulderlike feature at the maximum gap instead). For the surfaces in between {100} and {110}, we find that for the isotropic model the cusplike peak appears at the energy gap of the state with the momentum normal to the surface. This finding suggests the potential of the NIS tunneling spectroscopy as a tool to map out the magnitude of a *d*-wave gap function at different points on the Fermi surface. However, because this finding is based on the model that uses the assumption that the Fermi surface of the superconductor is isotropic, one has to be careful in applying the results to high-T_c cuprates. Angle-resolved photoemission spectroscopy (ARPES) measurements[21–24] show that the Fermi surfaces of these materials are far from being isotropic. They are however well described by a tight-binding model.

In order to better understand the tunneling conductance spectra of high-T_c cuprates, in this paper we use a lattice model that allows us to mimic the Fermi surfaces of the superconductors. In particular, we use a two-dimensional (2D) square lattice model in which the copper oxide planes of the superconductors are represented by a square lattice. We apply this model to examine the dependence on the surface orientation of the ab-plane tunneling conductance spectrum of a BCS $d_{a^2-b^2}$-wave superconductor using the BTK formalism.

The outline of this paper is as follows. Before we give the details of the formalism and results for the 2D lattice model, we review in the next section the results from the 2D isotropic model for later comparison. We explain why, in the isotropic model, the state with the momentum normal to the surface is the main contributor to the cusplike peak in the

tunneling conductance spectrum of the junction with orientations away from {100} and {110}. In Sec. III, we describe briefly the discrete lattice BdG equations and the formalism used to calculate the differential conductance. We also introduce the use of the surface-adapted Brillouin zone (SABZ) to obtain the right number of transmitted excitations, the linear combination of which is the wave function of the superconductor. In Sec. IV, we discuss the results from the lattice model. We then draw conclusions in Sec. V.

Throughout this article, we assume a spatially constant $d_{a^2-b^2}$-wave superconducting gap function for simplicity. The self-consistent solution of the gap function will give a correction of the order of the ratio of the maximum gap to the energy bandwidth of the superconductor. We neglect terms of this order in all the calculations in this work.

II. CONDUCTANCE SPECTRA FROM THE ISOTROPIC MODEL

Before discussing the tunneling conductance spectrum of a normal-metal-insulator-$d_{a^2-b^2}$-wave superconductor (NID) junction computed for the 2D lattice model, it is useful to consider in more detail the conductance of the 2D isotropic model to give an introduction and later a comparison. Quantitative calculations of the conductance have in fact already been carried out for this model in Ref. 7. Our aim in this calculation is to look at the individual contributions to the conductance in more detail, and to show why the cusplike feature occurs at the energy gap of the state with the momentum normal to the surface.

The isotropic model makes use of the assumption that the electronic structure of the *d*-wave superconductor is isotropic. The insulating layer of the NID junction in this model is represented by a delta-function potential of strength H.[7] The pairing potential is assumed to be zero in the normal metal and to be spatially constant with a $d_{a^2-b^2}$-wave symmetry in the superconductor. The geometry of the junction is displayed in Fig. 1. The conductance spectrum of the NID junction is found by using the BTK formula.[7,17] This model is able to capture most of the qualitative characteristics of the tunneling conductance spectrum of a *d*-wave superconductor.

Figure 2(b) shows the plots of normalized conductances of four junctions of different surface orientations (see also Ref. 7). Each surface orientation is characterized by α, an angle between the *a* axis of the superconductor and the surface normal of the junction [see Fig. 2(a)]. For $\alpha=0$ which corresponds to a {100} junction, the conductance spectrum is linear at low voltages and peaks at the voltages that correspond to the maximum energy gap. For $\alpha=\pi/4$ which corresponds to a {110} junction, the conductance spectrum contains a ZBCP and shoulderlike features at the maximum gap. For orientations between {100} and {110}, the conductance spectrum shows both the ZBCP with the shoulderlike feature and the cusplike peaks. As indicated by the arrows in Fig. 2(b), these cusplike peaks do not occur at the voltages corresponding to the maximum gap. As mentioned above, these peaks are in fact at the voltages corresponding to the energy gap of the state whose momentum is perpendicular to the surface.

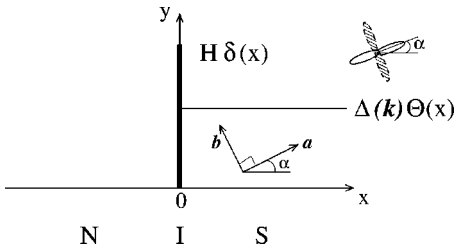

FIG. 1. The illustration of the NIS junction used in the isotropic model. The superconductor crystallographic orientation is characterized by α, an angle between the *a* axis and the *x* axis. The insulator is described by δ-function potential of strength *H*. $\Delta(\mathbf{k})\Theta(x)$ is the gap function. $\Theta(x)$ is a Heaviside-step function.

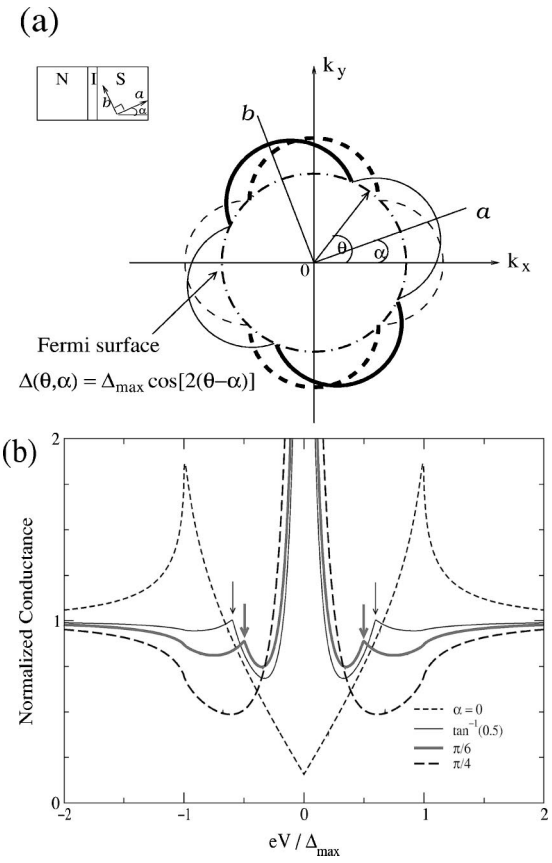

FIG. 2. (a) Schematic illustration of the Fermi surface (dash-dotted circle) and the gap function used in Ref. 7. The dashed curves represent the gap function when the *a* axis is along the *x* axis and the solid curves when the *a* axis is tilted with an angle α from the *x* axis. θ gives the direction of a Fermi wave vector. The gap function can be written as a function of the two angles: $\Delta(\theta,\alpha)=\Delta_{\max}\cos[2(\theta-\alpha)]$. (b) Plots of the conductance vs applied voltage of four junctions with different α. The parameters used in these plots (following the notation in Ref. 5) are $Z=1.5$ and $\lambda=1.0$. Note that cusplike peaks (indicated by the arrows) develop at $eV=\pm 0.6\Delta_{\max}$ for $\alpha=\tan^{-1}(0.5)$ and at $eV=\pm 0.5\Delta_{\max}$ for $\alpha=\pi/6$.

A. Conductance formula

In the isotropic model, the Fermi surfaces of both the normal metal and superconductor are assumed to be isotropic. The BdG equations used to describe the system are

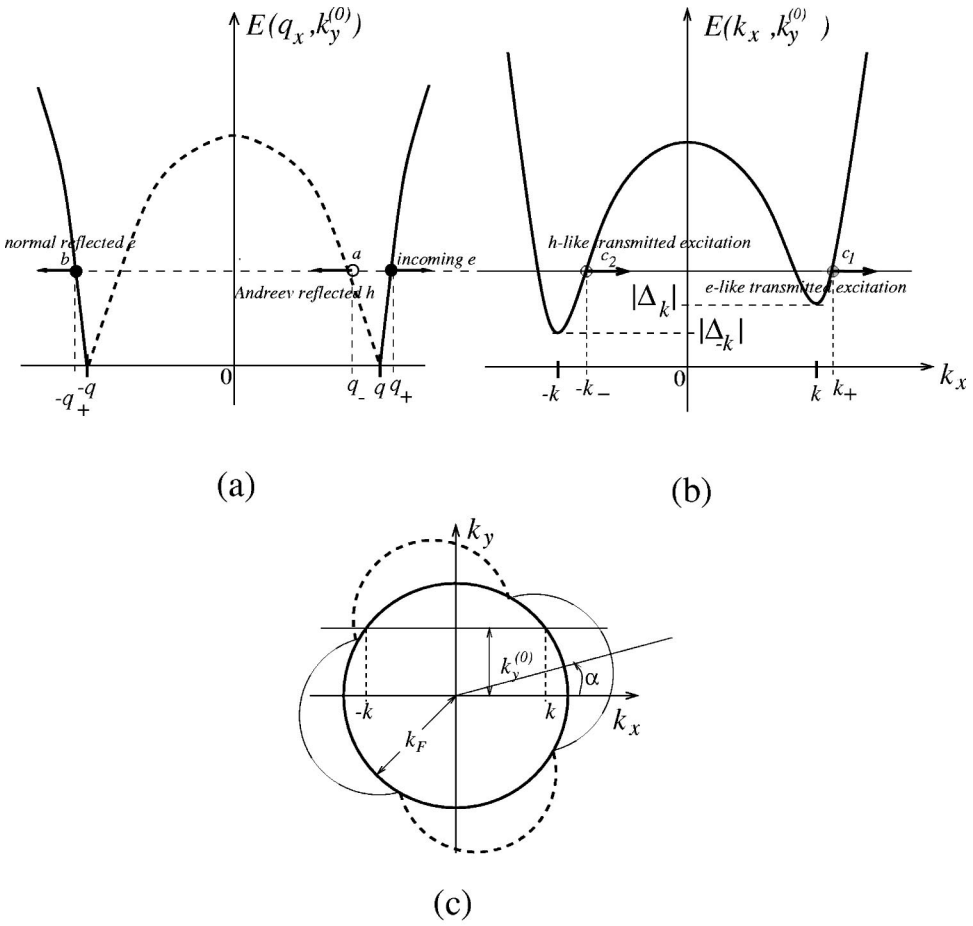

FIG. 3. The sketches of bulk quasiparticle energies of the normal metal (a) and the superconductor (b) at a given $k_y = k_y^{(0)}$. In (c), the Fermi surface of the superconductor, the a axis of which is tilted away from the x axis by an angle α, is shown. The dotted and solid curves outside the Fermi surface represent the $d_{a^2-b^2}$-wave gap function.

$$\begin{bmatrix} -\frac{\hbar^2}{2m}\nabla^2 - \mu & \Delta(\mathbf{x}) \\ \Delta^*(\mathbf{x}) & \frac{\hbar^2}{2m}\nabla^2 + \mu \end{bmatrix} U(\mathbf{x}) = E U(\mathbf{x}), \qquad (1)$$

where μ is the Fermi energy, m is the electron mass, $\Delta(\mathbf{x})$ is the pairing potential which is taken to be zero on the normal-metal side and spatially constant with a $d_{a^2-b^2}$-wave symmetry on the superconducting side, and $U(\mathbf{x})$ is a two-component wave function, the first and the second components of which are equivalent to electronlike and holelike excitations, respectively.

Assuming $U(\mathbf{x})$ takes the form $e^{i(q_x x + k_y y)}$, we obtain the bulk excitation energy of the normal metal as

$$E(q_x, k_y) = \pm\left[\frac{\hbar^2}{2m}(q_x^2 + k_y^2) - \mu\right], \qquad (2)$$

where q_x, k_y are x and y components of a wave vector. Note that the energy is always positive and the plus and minus signs correspond to the electron and hole energies, respectively. Figure 3(a) shows the sketch of the quasiparticle excitation energy in the bulk of the normal metal at a particular $k_y^{(0)}$, as indicated in Fig. 3(c). Treating an injected electron from the normal-metal side and using the fact that k_y is conserved, we write the wave function on the normal side as

$$U_N(x<0,y) = \left(\begin{bmatrix}1\\0\end{bmatrix} e^{iq_+ x} + a\begin{bmatrix}0\\1\end{bmatrix} e^{iq_- x} + b\begin{bmatrix}1\\0\end{bmatrix} e^{-iq_+ x}\right) e^{ik_y y}, \qquad (3)$$

where a, b are the Andreev and normal reflection amplitudes and $q_\pm$ satisfy Eq. (2) for electron and hole excitations at a particular k_y, respectively. $q_\pm$ are shown pictorially in Fig. 3(a).

Similarly, the quasiparticle energy in the bulk of the superconductor can be shown to be

$$E(k_x, k_y) = \sqrt{\xi_{\mathbf{k}}^2 + \Delta_{\mathbf{k}}^2}, \qquad (4)$$

where $\xi_{\mathbf{k}}$ is the normal-state energy,

$$\xi_{\mathbf{k}} = \frac{\hbar^2}{2m}(k_x^2 + k_y^2) - \mu \qquad (5)$$

and $\Delta_{\mathbf{k}}$ is the gap function,

$$\Delta_{\mathbf{k}} = \frac{\Delta_{\max}}{k_F^2}[(k_y^2 - k_x^2)\cos(2\alpha) + 2k_x k_y \sin(2\alpha)], \qquad (6)$$

where $k_F = \sqrt{2m\mu}/\hbar$ is the size of the Fermi wave vector in the superconductor. Figure 3(b) shows a sketch of the quasiparticle energy of the superconductor.

In general, for the junction orientation away from {100} and {110}, the magnitudes of the gaps of the states with $k_x = \pm k, \Delta_{\pm k} \equiv \Delta(\pm k, k_y)$ are not the same (except for $k_y = 0, k_F/\sqrt{2}$).

For each k_y, in the superconductor there are two transmitted excitations for all surface orientations, as depicted in Fig. 3(b). (In the lattice model as will be seen later, the number of the transmitted excitations depends on the surface orientation as well as the shape of the Fermi surface. It is not always two.) Therefore, the wave function of the superconductor is always a superposition of the two excitations,

$$U_S(x>0,y) = \left(c_1 \begin{bmatrix} u_{k_+} \\ v_{k_+} \end{bmatrix} e^{ik_+ x} + c_2 \begin{bmatrix} u_{-k_-} \\ v_{-k_-} \end{bmatrix} e^{-ik_- x} \right) e^{ik_y y}, \tag{7}$$

where c_1, c_2 are the transmission amplitudes, $k_\pm$ satisfy the energy Eq. (4) [shown pictorially in Fig. 3(b)], and u_k, v_k are defined as

$$u_k = \frac{E + \xi_k}{\sqrt{|E+\xi_k|^2 + |\Delta_k|^2}},$$

$$v_k = \frac{\Delta_k}{\sqrt{|E+\xi_k|^2 + |\Delta_k|^2}}.$$

Note that $|u_k|^2 + |v_k|^2 = 1$. The amplitudes a, b, c_1, and c_2 are found by using the matching conditions at the interface, which are

$$U_S(x=0^+) = U_N(x=0^-),$$

$$\left.\frac{\partial U_S}{\partial x}\right|_{x=0^+} - \frac{\partial U_N}{\partial x}_{x=0^-} = \frac{2mH}{\hbar^2} U_S(x=0^+). \tag{8}$$

Because the energies in which we are interested are $E \leqslant 2\Delta_{\max}$, which are a lot smaller than the Fermi energy, we will neglect the terms of order $\mathcal{O}(E/\mu)$. Within this approximation $q_- = q_+ = q$ and $k_- = k_+ = k$, where $q = \sqrt{q_F^2 - k_y^2}$ and $k = \sqrt{k_F^2 - k_y^2}$. For simplicity, we take $q_F = k_F$.

We defined a normalized conductance as the ratio of the NIS conductance to the conductance of the same junction but with the superconductor in the normal state, i.e.,

$$G(eV) \equiv \frac{G^{\mathrm{NIS}}(eV)}{G^{\mathrm{NIN}}(eV)}. \tag{9}$$

Following the formalism in Ref. 7, we obtain

$$G^{\mathrm{NIS}}(eV) = \frac{e^2}{h} \langle 1 + A(k_y, eV) - B(k_y, eV) \rangle_{k_y}, \tag{10}$$

$$G^{\mathrm{NIN}}(eV) = \frac{e^2}{h} \langle P(k_y) \rangle_{k_y}, \tag{11}$$

where A and B are the Andreev and normal reflection probabilities, respectively, $P \equiv 1 - B$ is the transmission probability across the insulating barrier when the superconductor is in the normal state [$A = 0$], and the angular brackets indicate an average over k_y. Both $1 + A - B$ and P can be interpreted as the number of the electrons crossing NIS and normal-metal-insulator-normal-metal (NIN) junctions for each incident electron, respectively. The normal reflection process reduces the number of the electrons crossing any junction, whereas the Andreev reflection process enhances it.[25] Thus, the value of $1 + A - B$ ranges from 0 to 2, whereas that of P ranges from 0 to 1.

B. Tunneling conductance spectrum for the NID{210} junction

The wave function of the superconductor in the isotropic model is a linear combination of two transmitted excitations. When $E < \min[|\Delta_{-k}|, |\Delta_k|]$, both excitations are exponentially decaying with the wave vectors $\pm k + i\mathcal{O}(|\Delta_{\pm k}|/\mu)$. These excitations make up a zero-energy surface bound state on the condition that the signs of both gaps are opposite.[8] In case of $\alpha = 0$, or a {100} interface, the signs of the two gaps are always the same; thus, no zero-energy bound states are formed and there is no ZBCP. The main feature in the conductance spectrum in this case is a V-shaped gaplike structure which varies linearly at low voltages and peaks at the voltages equivalent to $\pm\Delta_{\max}$. In the case of $\alpha = \pi/4$, or a {110} interface, the signs of the two gaps of the two excitations are different for all k_y. Thus, zero-energy bound states exist for all k_y and contribute to a ZBCP with shoulderlike features at the voltages equivalent to $\pm\Delta_{\max}$.

For the junction with $0 < \alpha < \pi/4$, only states with some k_y can become zero-energy surface bound states. Specifically, the zero-energy bound states are those with k_y in the range $k_F \sin(\pi/4 - \alpha) < |k_y| < k_F \sin(\pi/4 + \alpha)$. The ratio of the range of k_y that gives zero-energy surface bound states to the total number of k_y on the Fermi surface is equal to $\sqrt{2}\sin(\alpha)$. For a {210} surface, which is equivalent to $\alpha = \tan^{-1}(0.5)$, around 63% of k_y on the Fermi surface contributes to a ZBCP. Figure 4 shows the plots of the two gaps $\Delta_{\pm k}$ of the two transmitted excitations as a function of k_y in this case.

As shown in Fig. 2(b), for $\alpha = \tan^{-1}(0.5)$ there are symmetric cusplike peaks at $eV = \pm 0.60\Delta_{\max}$ in the conductance spectrum. To understand where these peaks come from, we consider the function $T(E, k_y) \equiv 1 + A(E, k_y) - B(E, k_y)$.

First, we discuss $T(E, k_y)$ for the states with k_y in the range that does not provide zero-energy surface bound states, e.g., $k_y = 0$, $\pm 0.1 k_F$, and $\pm 0.2 k_F$. As shown in Fig. 5, for $k_y = 0$, $T(E)$ is symmetric around zero energy. It contains a U-shaped gaplike feature with sharp peaks at $E = \pm\Delta(k_y = 0) = \pm 0.60\Delta_{\max}$.

For $k_y = \pm 0.1 k_F$, $\pm 0.2 k_F$ [see Fig. 6(a)], $T(E)$ is no longer symmetric. It still has a symmetric U-shaped gaplike feature, but with asymmetric broader shoulders, not as sharp as in the case of $k_y = 0$. The shoulders are different in height but the same in width (equal to the difference of the magnitude of the two gaps $|\Delta_k|, |\Delta_{-k}|$). The further $|k_y|$ is away from zero, the flatter and lower the shoulders become [compare Figs. 6(a) and 6(c)].

Because the conductance can be interpreted as the average of $T(E, k_y)$ over all k_y, the $k_y = 0$ state gives the conduc-

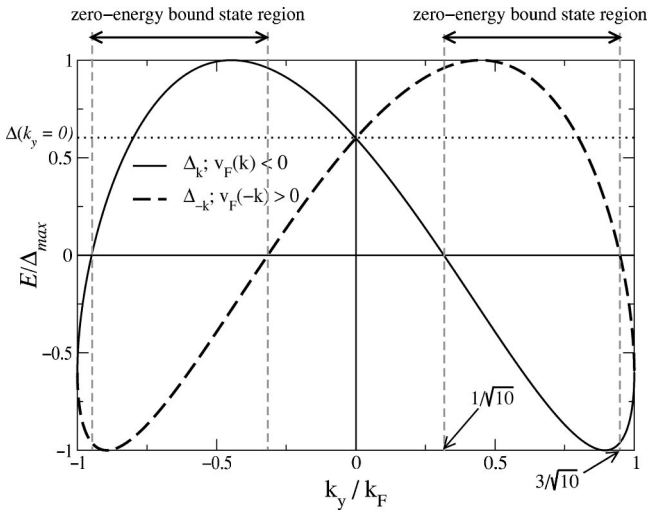

FIG. 4. Plots of Δ_{-k} and Δ_k as a function of k_y for an NID junction with $\alpha=\tan^{-1}(0.5)$. Only states with $k_F/\sqrt{10}<|k_y|<3k_F/\sqrt{10}$ contribute to a ZBCP. The states with k_y outside this region give rise to cusplike peaks at $eV=\pm 0.60\Delta_{\max}$. Note that $v_F \equiv d\xi_{\mathbf{k}}/dk_x$.

tance spectrum cusps at $eV=\pm\Delta(k_y=0)=\pm\Delta_{\max}\cos(2\alpha)$. Note that in spite of the asymmetry of $T(E)$ at each $k_y\neq 0$, the resulting conductance curve is symmetric. The reason is that for every $T(E,k_y\neq 0)$ there is a $T(E,-k_y)$ that has the counteracting asymmetry, e.g., compare Figs. 6(a) and 6(b). When these two add up, they give the symmetric result.

Now consider $T(E,k_y)$ in the region of k_y for which zero-energy bound states can be formed. For instance, $k_y=\pm 0.4k_F$, $\pm 0.6k_F$. Figure 7 shows plots of $T(E)$ for these k_y. All plots display symmetric Lorentzian-like peaks centered at zero energy. The peak width is determined by the smaller gap of the two transmitted excitations. At an energy equal to the larger gap, there is a noticeable feature. Like the states that do not contribute to a ZBCP, $T(E,k_y)$ is not symmetric. However, for each asymmetric $T(E,k_y)$, there is $T(E,-k_y)$ that has the counteracting asymmetry. Thus, the summation of all these pairs leads to symmetry in the conductance spectrum.

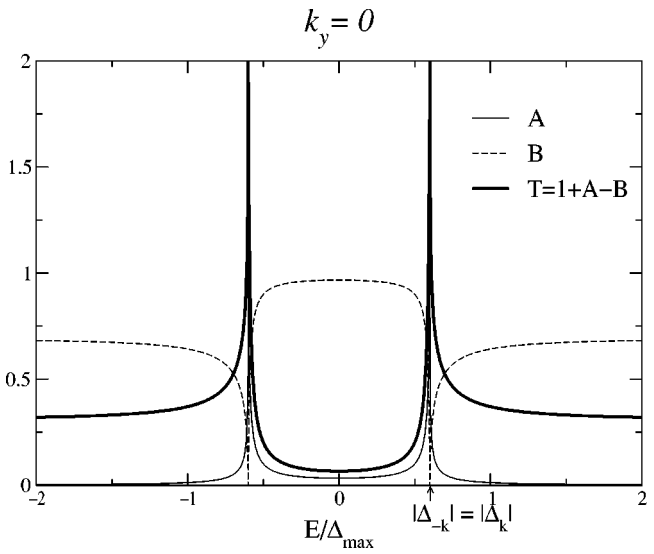

FIG. 5. The plots of A, B, and T for $\alpha=\tan^{-1}(0.5)$ and $k_y=0$.

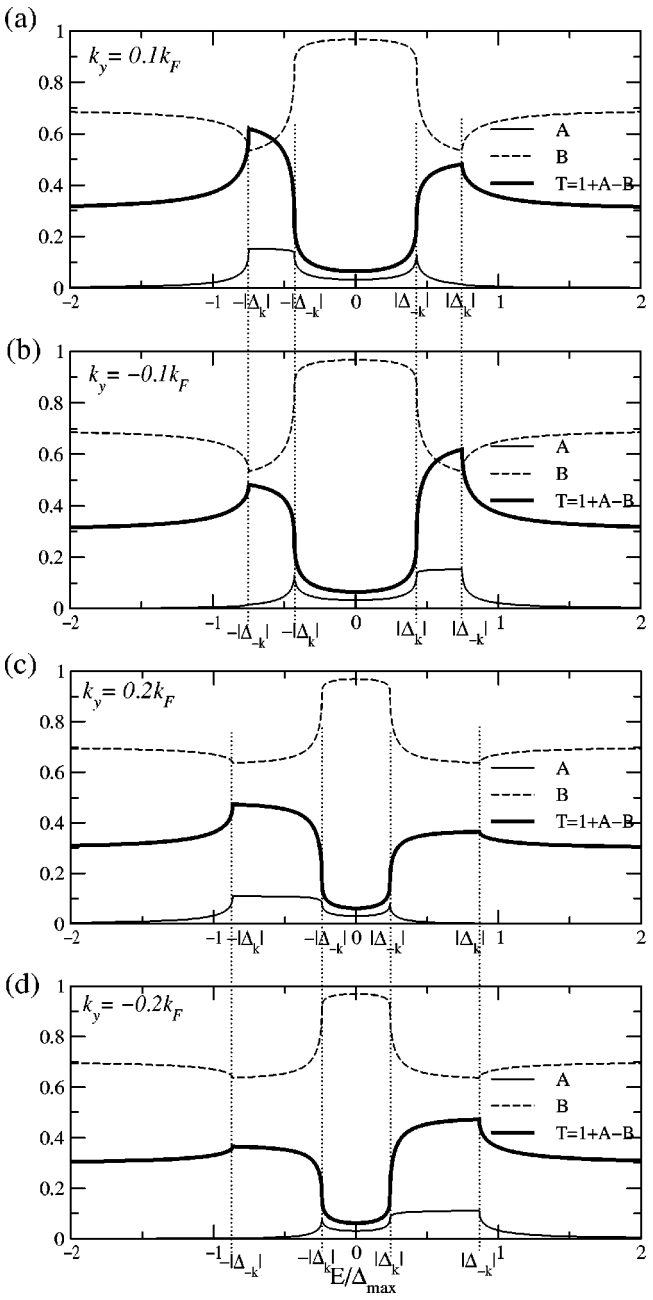

FIG. 6. The plots of A, B, and T for $\alpha=\tan^{-1}(0.5)$ at four k_y's in the region where zero-energy surface bound states are not formed. The largest asymmetry in T occurs when $\min[|\Delta_{-k}|,|\Delta_k|]<|E|<\max[|\Delta_{-k}|,|\Delta_k|]$. The asymmetry comes from A, not B.

In summary, the isotropic model gives us relatively simple predictions for the features of the ab-plane tunneling conductance spectrum of a $d_{a^2-b^2}$-wave superconductor. For the junction with orientation away from {100} and {110}, the spectrum is symmetric and contains a ZBCP, a shoulderlike feature at the maximum gap, and cusplike peaks at the voltages equivalent to the energy gap of the state with the momentum normal to the surface.

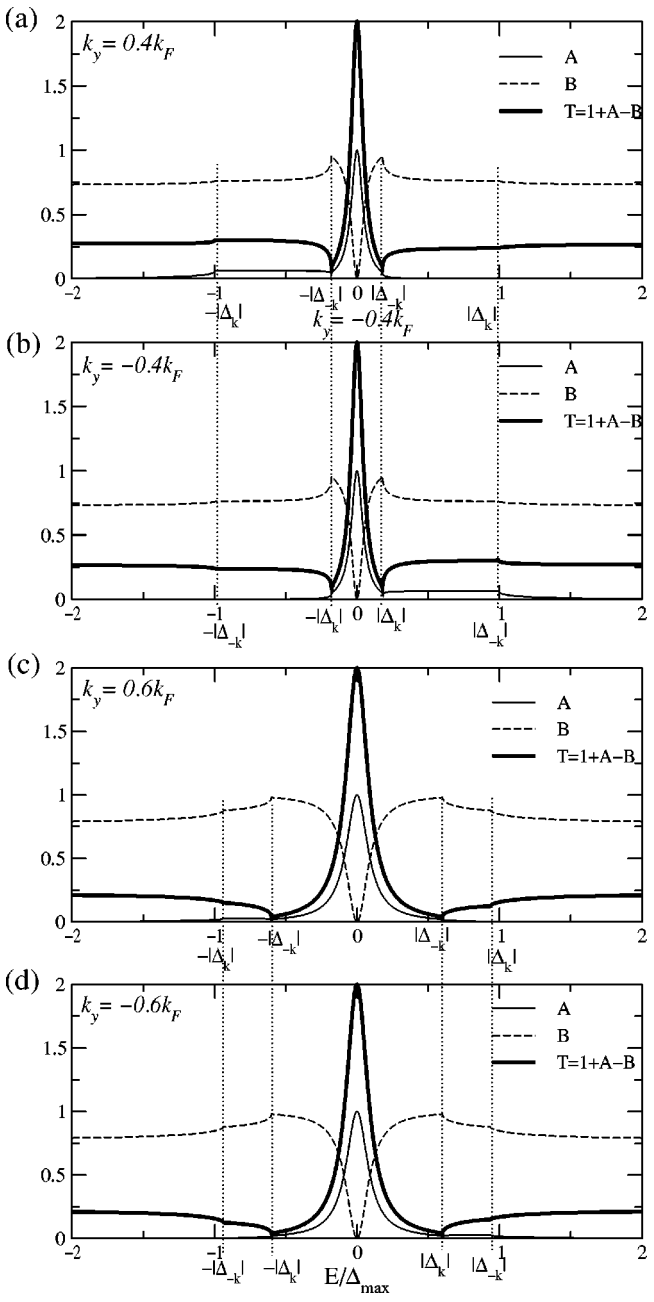

FIG. 7. The plots of A, B, and T for $\alpha = \tan^{-1}(0.5)$ at four k_y's in the region where zero-energy Andreev bound states can be formed. The largest asymmetry in T occurs when $\min[|\Delta_{-k}|,|\Delta_k|] < |E| < \max[|\Delta_{-k}|,|\Delta_k|]$, and it comes from A only.

III. 2D LATTICE MODEL AND CONDUCTANCE FORMULA

In this section, we introduce the 2D lattice model. We represent our ab-plane NID junctions with infinite 2D square lattices. Three examples of different superconductor surface orientations are depicted in Fig. 8. Note that for simplicity we keep the normal metal oriented in the {100} direction.

We describe our system by the following 2D discrete Bogoliubov–de Gennes equations,[26,27]

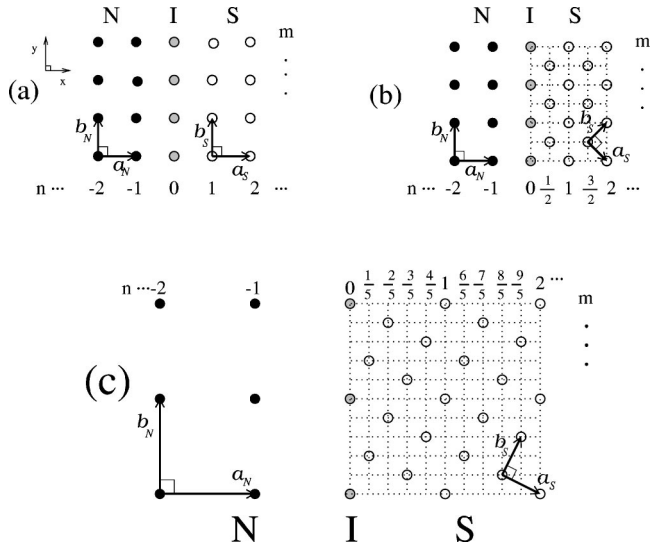

FIG. 8. 2D lattice networks used to represent (a) {100}, (b) {110}, and (c) {210} junctions. The solid, grey, and open circles represent normal-metal, insulator, and superconductor layers, respectively. $\boldsymbol{a}_i$ and $\boldsymbol{b}_i$, where $\boldsymbol{i}$ is $\boldsymbol{N}$ (normal metal) or $\boldsymbol{S}$ (superconductor), are the crystallographic basis vectors.

$$\sum_{\mathbf{x}'} \begin{bmatrix} -t(\mathbf{x},\mathbf{x}') & \Delta(\mathbf{x},\mathbf{x}') \\ \Delta^*(\mathbf{x},\mathbf{x}') & t(\mathbf{x},\mathbf{x}') \end{bmatrix} U(\mathbf{x}') = EU(\mathbf{x}), \tag{12}$$

where $U(\mathbf{x})$ is a two-component wave function and $\mathbf{x}$ labels the ion positions. The summation is carried over the nearest-neighbor sites and may also include next-nearest sites.

On the normal-metal side, there is no gap function, i.e., $\Delta(\mathbf{x},\mathbf{x}')=0$, and for simplicity we assume there are only nearest-neighbor hoppings, i.e., the only nonzero $t(\mathbf{x},\mathbf{x}')$ are $t(\mathbf{x},\mathbf{x}\pm\boldsymbol{a}_N)=t_N>0$; $t(\mathbf{x},\mathbf{x}\pm\boldsymbol{b}_N)=t'_N>0$. On the superconducting side, we define the hopping terms as follows: $t(\mathbf{x},\mathbf{x}\pm\boldsymbol{a}_S)=t(\mathbf{x},\mathbf{x}\pm\boldsymbol{b}_S)=t_S>0$; $t(\mathbf{x},\mathbf{x}\pm\boldsymbol{a}_S\pm b_S)=-t'_S\leq 0$. The gap function on this side is taken to be $d_{a^2-b^2}$ wave: $\Delta(\mathbf{x},\mathbf{x}\pm\boldsymbol{a}_S)=-\Delta(\mathbf{x},\mathbf{x}\pm\boldsymbol{b}_S)=\Delta$.

Because every lattice system considered here is invariant with respect to a translation parallel to the surface through a distance a_N (a lattice constant of the normal metal), the component along the surface (k_y) of a momentum $\mathbf{k}$ is conserved within a reciprocal-lattice vector corresponding to the translation $a_N = a_S\sqrt{h^2+k^2}$, where $\{hk0\}$ are integers that specify the orientation of the superconductor for ab-plane junctions. This range of k_y within which the momentum $\mathbf{k}$ is conserved will specify the shape of the SABZ for each surface orientation. Because the SABZ has the same area as the bulk BZ, the range of k_x has to be $2\pi\sqrt{h^2+k^2}/a_S$ long. The surface states of each surface orientation are basically the superpositions of the bulk states. The SABZ is used to specify which bulk states will contribute to each surface state of that orientation, that is, it is composed of the states of the same k_y in that SABZ.

From Bloch's theorem, the eigenstates of Eq. (12) therefore can be written as

$$U(\mathbf{x}) = e^{imk_y a_N} U^{k_y}(n), \tag{13}$$

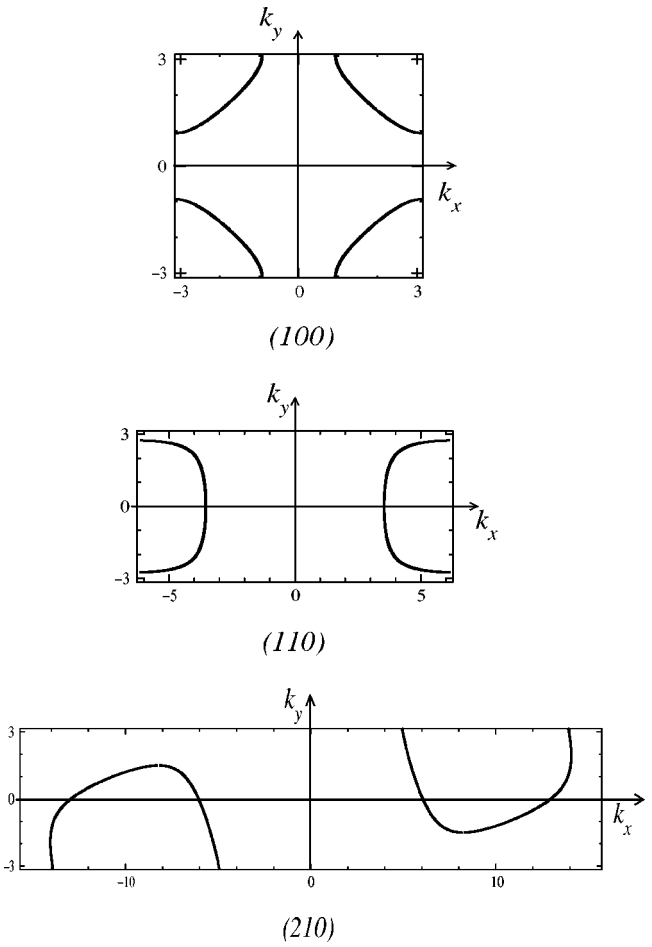

FIG. 9. The SABZ's for three surface orientations: {100}, {110}, and {210}. For each Brillouin zone (BZ), we draw a Fermi surface that corresponds to a little more than a half-filled band with nearest-neighbor interactions.

where m,n are ionic row and column indices as indicated in Fig. 8. Substituting $U(\mathbf{x})$ into Eq. (12), we can reduce Eq. (12) to a 1D eigenvalue equation

$$\sum_{n'} T^{k_y}(n,n')U^{k_y}(n') = EU^{k_y}(n) \tag{14}$$

for each k_y. $T^{k_y}(n,n')$ is the appropriate (2×2) energy matrix between two ions with column indices n and n'. Equation (14) describes the excitations in the bulk state of each side and also provides us with the matching conditions for the two wave functions at the interface.

The wave function describing each side of the junction is a linear combination of the appropriate excitations of the same energy and k_y. The number of the excitations depends on the shape of Fermi surface and the SABZ. Figure 9 shows three SABZ's of the superconductor with different orientations. Because we assign the normal side to have a {100} surface, its SABZ is the same as the bulk BZ, which is a $(2\pi/a_N \times 2\pi/a_N)$ square. The shape of SABZ of the superconductor, however, is not always a square. For an $\{hk0\}$ interface, the SABZ is a $[2\pi/(a_S\sqrt{h^2+k^2}) \times 2\pi\sqrt{h^2+k^2}/a_S]$ rectangle, which still has the same area as the bulk BZ. The difference in shape of the SABZ has an impact on the number of the quasiparticle excitations that make up the wave function of the superconductor.

Writing $U_N^{k_y}(n) = Ce^{iq_x m a_N}$ and substituting it into Eq. (14), we obtain the normal side bulk quasiparticle energy as

$$E(q_x,k_y) = \pm[\epsilon_N - \mu - 2t_N\cos(q_x a_N) - 2t_N'\cos(k_y a_N)], \tag{15}$$

where ϵ_N is the normal-metal on-site energy and $|q_x| < \pi/a_N$.

The bulk quasiparticle energy of the superconductor is

$$E(k_x,k_y) = \sqrt{\xi_{\mathbf{k}}^2 + \Delta_{\mathbf{k}}^2}, \tag{16}$$

where

$$\xi_{\mathbf{k}} = \epsilon_S - \mu - 2t_S\left[\cos\left(\frac{hk_x+kk_y}{\sqrt{h^2+k^2}}a_S\right) + \cos\left(\frac{kk_x-hk_y}{\sqrt{h^2+k^2}}a_S\right)\right] + 2t_S'\left[\cos\left(\frac{(h+k)k_x+(h-k)k_y}{\sqrt{h^2+k^2}}a_S\right) + \cos\left(\frac{(h-k)k_x-(h+k)k_y}{\sqrt{h^2+k^2}}a_S\right)\right], \tag{17}$$

$$\Delta_{\mathbf{k}} = 2\Delta\left[\cos\left(\frac{hk_x+kk_y}{\sqrt{h^2+k^2}}a_S\right) - \cos\left(\frac{kk_x-hk_y}{\sqrt{h^2+k^2}}a_S\right)\right], \tag{18}$$

and $|k_x| < \pi\sqrt{h^2+k^2}/a_S$.

Now we consider the wave function for each region that satisfies Eq. (14). Treating an injected electron from the normal side, we write the normal-metal wave function $U_N^{k_y}$ as a summation of three excitations as in the isotropic model,

$$U_N^{k_y}(n\leqslant 0) = \begin{bmatrix}1\\0\end{bmatrix}e^{iq_+ a_N n} + a\begin{bmatrix}0\\1\end{bmatrix}e^{iq_- a_N n} + b\begin{bmatrix}1\\0\end{bmatrix}e^{-iq_+ a_N n}. \tag{19}$$

The x components of the wave vectors $q_\pm$ satisfy Eq. (15) at a particular k_y.

The wave function of the superconducting region can be written as

$$U_S^{k_y}(n>0) = \sum_m c_m U_S^{k_y,m}(n), \tag{20}$$

where the summation is over all the transmitted quasiparticle excitations and c_m is a transmission amplitude. The number of the transmitted excitations depends on the shape of the Fermi surface as well as the surface orientation. For example, a system with a {210} surface and a Fermi surface as shown in Fig. 9 can have in the normal state four real-k_x excitations for some k_y on the Fermi surface. This means there can be eight quasiparticle excitations in the superconducting state at that k_y; however, only four of them are transmitted excitations (i.e., their group velocities are away from the junction). Each excitation takes the following form:

$$U_S^{k_y,m}(n)=\begin{bmatrix} u_{k_m^{\pm}} \\ v_{k_m^{\pm}} \end{bmatrix} e^{ik_m^{\pm}a_S\sqrt{j^2+k^2}n}, \tag{21}$$

where $k_m^{\pm}$ are the x components of the wave vectors that satisfy Eq. (16) ($\pm$ correspond to either an electronlike or a holelike excitation). Each of a, b and all the c_m can be found as a function of E and k_y by matching $U_N^{k_y}$ and $U_S^{k_y}$ at the interface according to Eq. (14). Note that because the number of quasiparticle excitations is conserved, all the reflection and transmission probabilities will add up to unity. This conservation as well as the conservation of the electric current at the interface is used as a check of all the numerical calculations in this work.

Following the BTK formalism,[17] we obtain the normalized differential conductance at zero temperature as

$$G(eV)=\frac{\langle 1+A(k_y,eV)-B(k_y,eV)\rangle_{k_y}}{\langle P(k_y)\rangle_{k_y}}. \tag{22}$$

It is noteworthy that Eq. (22) works for both positive and negative applied voltage. For the positive applied voltage, the expressions for a and b are evaluated by assuming an incoming electron as described above. For the negative voltage, the coefficients are calculated by assuming an incoming hole instead. It should be mentioned that because $\Delta_{\max} \leqslant 0.2t_S$ in high-T_c materials[4] and because we are interested in the energies E less than $2\Delta_{\max}$, we ignore all terms of order $\mathcal{O}(E/t_S)$ in all the calculations throughout this article. This approximation leads to $q_+=q_-=q$, where q satisfies Eq. (15) with $E=0$, and $|k_m^+|=|k_m^-|=|k_m|$, where all k_m satisfy Eq. (16) for $\xi_{\mathbf{k}}=0$. Also, $\Delta_{k_m^{\pm}}=\Delta_{k_m}$ and $\xi_{k_m^{\pm}}=\pm\sqrt{E^2-\Delta_{k_m}^2}$.

IV. CONDUCTANCE SPECTRA FROM THE 2D LATTICE MODEL

We now examine the effect of the anisotropic Fermi surface on the tunneling spectra of NID junctions using the lattice model. We will consider both nearest- and next-nearest-neighbor approximations. And to ensure that all the peaks and humps in the conductance spectra come from the superconductor and not the normal metal, we assign the following properties to the normal metal. We take the normal-metal crystal to be aligned in a specific orientation, which is {100}. We also take the energy bandwidth of the normal metal to be an order of magnitude larger than that of the superconductor. This describes the situation in most tunneling experiments with high-T_c materials. We let the hopping energy along the surface be ten times smaller than that normal to the surface ($t_N'=0.1t_N$) and the Fermi surface of the normal metal is at a half-filled band, which is characterized by a parameter $\nu_N\equiv(\mu-\epsilon_N)/[2(t_N+t_N')]=0$. (This Fermi surface is shown as the thickest energy contour line in Fig. 10.) These conditions are for simplicity, to ensure that there will be quasiparticles available for tunneling into the superconductor at all k_y, and that the DOS of the normal metal as a function of k_y is featureless, or close to being independent of k_y.

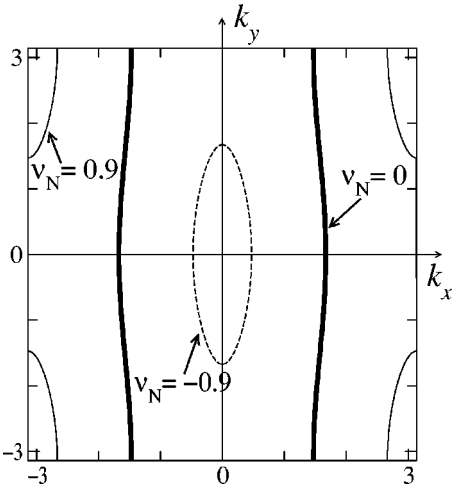

FIG. 10. Three Fermi levels of the normal metal with $t_N'=0.1t_N$. The parameter ν_N, which is defined in the text, specifies the Fermi level. Here, we use k_x and k_y in place of k_xa_N and k_ya_N.

For the superconductor, we consider two approximations: nearest- and next-nearest neighbor. For the nearest-neighbor approximation, we assign the following parameters: $t_S'=0$, $t_S=t_N'=10\Delta_{\max}$. The choice of the parameter t_S in fact does not affect the main results of the tunneling conductance spectra, as long as $t_S\gg\Delta_{max}$. For the next-nearest-neighbor approximation, we take $t_S'=0.45t_S$ so as to reproduce qualitatively the CuO_2 plane Fermi surface of $YBa_2Cu_3O_{7-\delta}$ as deduced by ARPES measurements.[22–24] The Fermi surface is characterized by a parameter $\nu_S\equiv(\mu-\epsilon_S)/(4t_S)$. Different Fermi surfaces in each approximation are shown in Fig. 11.

We take the barrier strength on the insulating layer to be zero for simplicity, because even without a potential barrier we are still in the tunneling limit with those parameters defined above. That is, the mismatch of the group velocities of the incoming and transmitted excitations acts as a large effective barrier.

A. Nearest-neighbor interactions

In this approximation, we consider the case of the {210} surface orientation, as an example of the orientations away

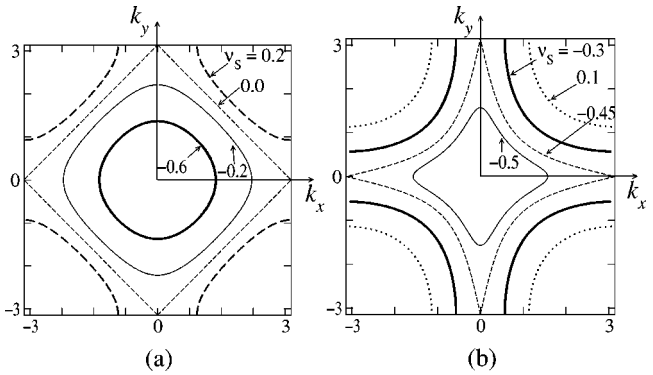

FIG. 11. (a) Four Fermi levels used in the nearest-neighbor approximation case and (b) in the next-nearest-neighbor approximation case.

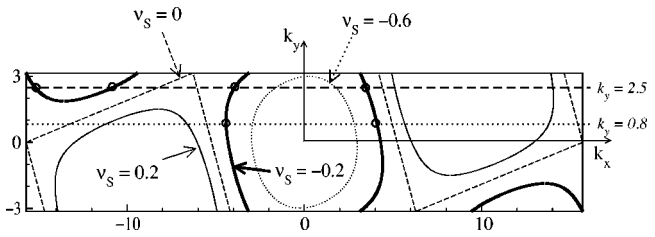

FIG. 12. The SABZ for the {210} case. The contour lines inside the BZ represent Fermi surfaces as parametrized by different ν_S.

from {100} and {110}. Both conductance spectra of {100} and {110} surfaces are similar to those in the isotropic model; therefore, we will not discuss them here.

Unlike in the isotropic model, the {210} case in the lattice model involves the states which are linear combinations of the four transmitted excitations of the same energy and k_y. This changes the condition in which a zero-energy surface bound state is formed. As a result, the range of k_y that contributes to such bound states varies with the shape of the Fermi surface. The isotropic model predicts that the range of k_y that contributes to a ZBCP is around 63% of all k_y in a BZ. In the lattice model with nearest-neighbor approximation, this range varies from zero to around 63%.

The superconductor wave function of the {210} case is written as a summation of four transmitted excitations:

$$U_S^{k_y}(n>1)=\sum_{j=1}^{4} c_j \begin{bmatrix} u_{k_j} \\ v_{k_j} \end{bmatrix} e^{ik_j a_S \sqrt{5} n}, \tag{23}$$

where $k_j, j=1 \ldots 4$ are k_x of the wave vectors that satisfy $\xi_{\mathbf{k}}=0$ for each k_y. k_j are, in general, complex. For instance, in Fig. 12 the lines of $k_y=2.5$ and $k_y=0.8$ cut the Fermi surface of $\nu_S=-0.2$ at different numbers of points, which represent the real solutions in each case.

Whether or not each $U_S^{k_y}$ can be a zero-energy surface bound state depends on the following conditions. If only two of the four excitations have real k_x, a zero-energy surface bound state will be formed if the gaps of the two propagating excitations have opposite signs. In the case in which all four excitations have real k_x, a zero-energy bound state is formed, when the two excitations with their Fermi velocities $v_F=d\xi_{\mathbf{k_F}}/dk_x$ of the same sign have gaps of the same sign which must be opposite to one of the gaps of the remaining two excitations. We plot the gaps of the propagating excitations as a function of k_y for various Fermi surfaces in Fig. 13. The dashed and solid curves in Figs. 13(a)–13(c) represent the gaps as a function of k_y of the excitations with positive and negative v_F, respectively.

For a Fermi surface corresponding to a half-filled band ($\nu_S=0$), the states of all k_y in the BZ consist of four transmitted excitations whose k_x are real. However, because the condition for a zero-energy surface bound state to be formed is not met at any k_y, no such bound states can exist. The conductance spectrum in this case, therefore, does not contain a ZBCP, as shown in Fig. 14. The spectrum is symmetric around zero applied voltage and contains a V-shaped gaplike feature that peaks at $\pm 0.50\Delta_{\max}$. At $eV=\pm\Delta_{\max}$, there are also less prominent features, shown in the right inset of Fig. 14. The disappearance of the ZBCP in the half-filled band case is consistent with the calculated local DOS of a 1×2 zigzag surface in Ref. 27.

To understand why the {210} tunneling conductance spectrum from the lattice model peaks at $\pm 0.50\Delta_{\max}$, consider again the plots of the function $T(E)$ for various k_y. For $k_y=0$, there are only two values of the gaps: $0.50\Delta_{\max}$ and $\Delta_{\max}$ [see Fig. 13(a)]. The plot of $T(E)$ at this k_y shows symmetry around zero energy. It peaks at its maximum value at $E=\pm 0.50\Delta_{\max}$. There is no feature at Δ_{max} because the excitations having this value of the gap have zero Fermi

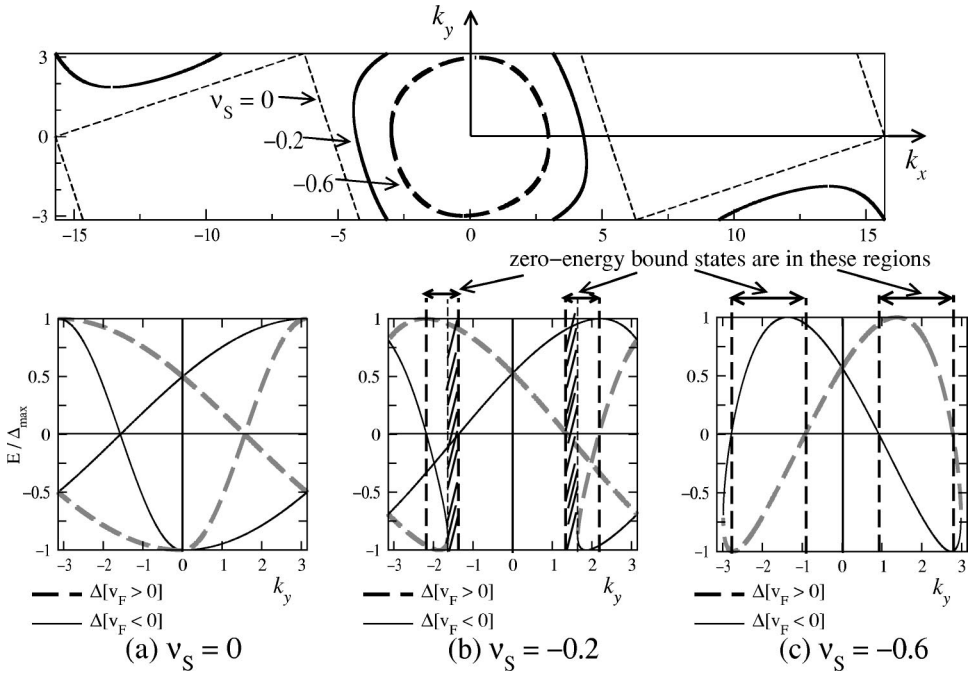

FIG. 13. Plots of the gap functions for propagating excitations in three cases: $\nu_S=0$, -0.2, and -0.6. For $\nu_S=0$, there are no regions in which zero-energy bound states exist. The region gets bigger when the Fermi surface is away from $\nu_S=0$. The shadowed region is the region where only two out of four excitations, which make up zero-energy bound states, have real k_x.

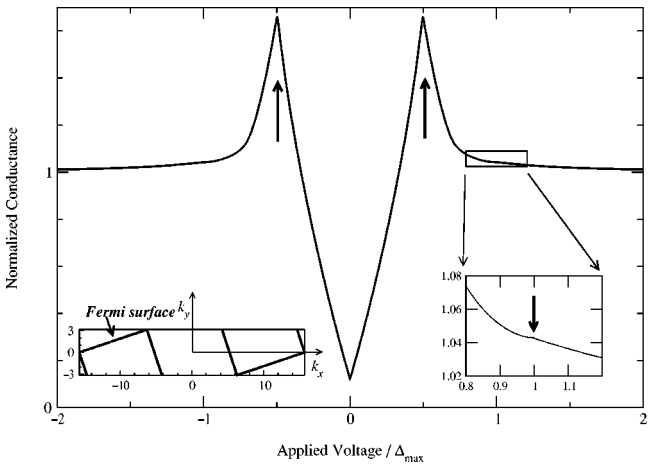

FIG. 14. Tunneling conductance spectrum of an NID{210} junction with the superconductor having a half-filling Fermi surface (the left inset). The right inset is an enlarged plot at the voltages near $\Delta_{\max}$. Note that the cusplike peaks are not at $\pm\Delta_{\max}$.

velocities. For $k_y \neq 0$, the function $T(E)$ is no longer symmetric. It still contains a symmetric U-shaped gaplike feature, but with asymmetric shoulders. The width of the U-shaped feature is governed by the minimum magnitude among the four gaps. Also, as depicted in Figs. 15(b)–15(e), there are four distinct features at energies equal to the magnitudes of the four gaps at that particular k_y.

Because the normalized tunneling conductance is basically a summation of functions $T(E,k_y)$ over all k_y in the SABZ, the resulting conductance curve of this case contains a V-shaped gaplike feature (due to the average of different U-shaped features over all k_y) that peaks at voltages $\pm\Delta(k_y=0)=\pm 0.50\Delta_{\max}$ and has no ZBCP. Note that even though each $T(E,k_y\neq 0)$ is asymmetric, the resulting conductance spectrum in this case is still symmetric because for each $T(E,k_y\neq 0)$ there is a $T(E,k_y-\pi)$ that has a counteracting asymmetry [compare Figs. 15(b) and 15(e), as well as 15(c) and 15(d)]. In fact, the case of the half-filled band proves to have special symmetry, i.e., it sits at the van Hove singularity which is a symmetric DOS point in the normal state. The number of the filled states (electron states) is exactly the same as that of the empty states (hole states). For any other case, which is not a half-filled band and in which the states are composed of four excitations with real k_x, for any $T(E,k_y)$ there will no longer exist a counteracting asymmetric $T(E,k_y')$, and this will lead to an asymmetric conductance spectrum.

For a Fermi surface with $\nu_S=-0.2$, some states consist of four excitations with real k_x, whereas the rest are the summations of four excitations, only two of which having real k_x. The region of k_y that gives zero-energy surface bound states is indicated by the arrows in Fig. 13(b). The region is also divided into two groups:

1. The region in which k_y gives the states that are made up of four real-k_x excitations. This region is in the unshadowed areas.

2. The region in which k_y gives the states that are made up of four excitations, only two of which having real k_x. This region is in the shadowed areas.

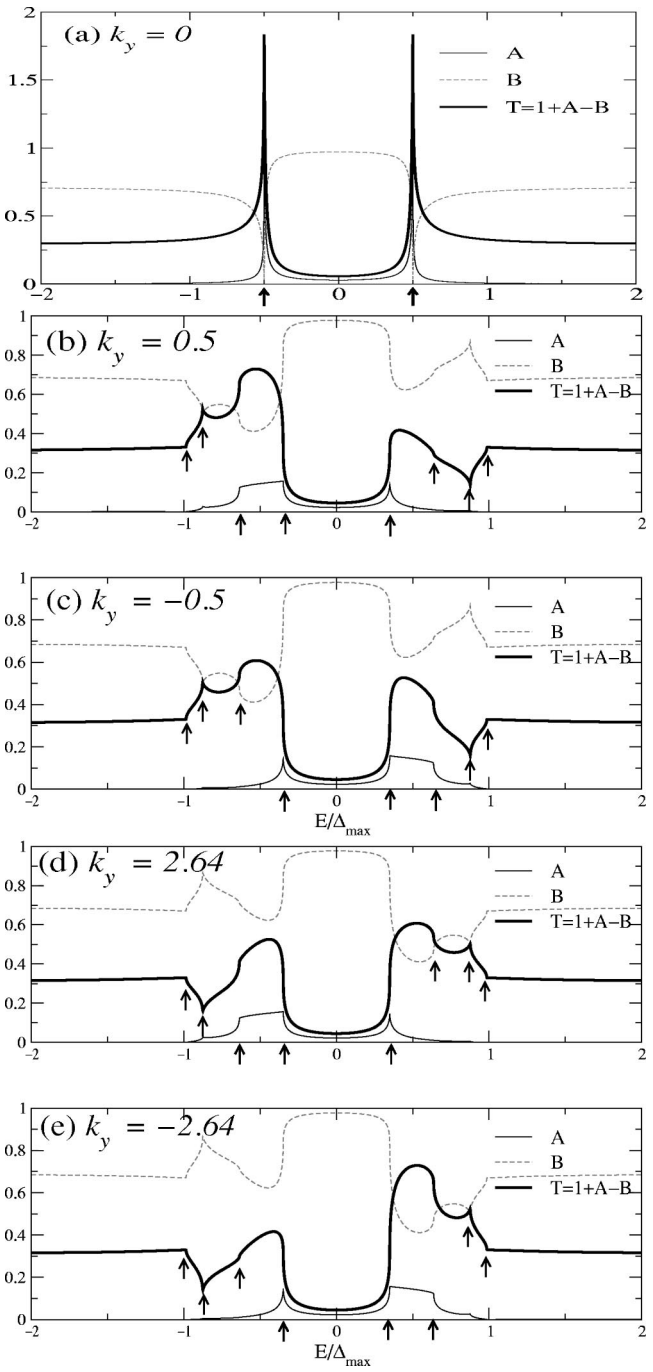

FIG. 15. Plots of $A(E)$, $B(E)$, and $T(E)$ in a {210} case with a half-filled band at various values of k_y.

The region of k_y that provides zero-energy surface bound states in this case is around 25% of all k_y in the BZ. Therefore, in addition to a V-shaped gaplike feature which is still apparent, the tunneling conductance spectrum contains a ZBCP as shown in Fig. 16. Although the position of the gaplike peaks are symmetric in energy (at $\pm 0.52\Delta_{\max}$) their heights and shapes are asymmetric. The energy $0.52\Delta_{\max}$ is in fact the value of the gap of the state with $k_y=0$, the same as in the case of $\nu_S=0$.

For the states with k_y in the region where the states are made up of four excitations, only two of which having real

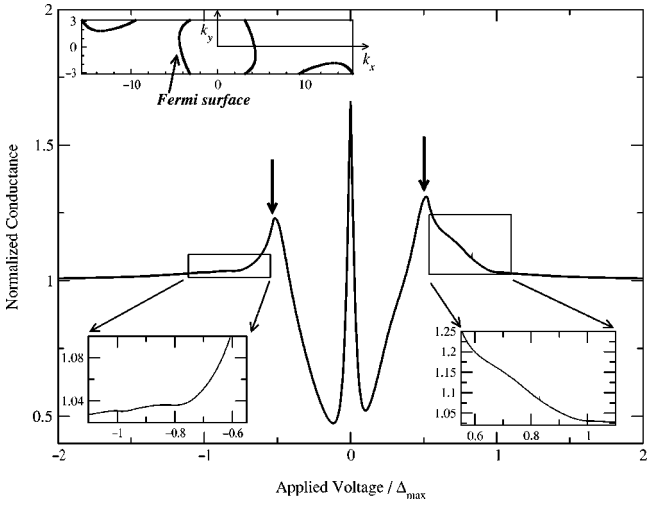

FIG. 16. The tunneling conductance spectrum of an NID{210} junction with the superconductor having a $\nu_S=-0.2$ Fermi surface (the upper left inset). The lower insets are enlarged plots at the voltages near $\Delta_{\max}$.

k_x, $T(E,k_y)$ behaves as in the isotropic model. That is, $T(E,k_y)$ of these states has a counteracting asymmetry to $T(E,-k_y)$. Thus, they are not responsible for the asymmetry in the conductance spectrum.

Figure 17 displays a few plots of $T(E)$ as well as $A(E)$ and $B(E)$ for the states which consist of four real-k_x excitations and cannot become zero-energy bound states. $T(E)$ in this case shows a U-shaped gaplike feature with the asymmetric peaks at an energy slightly below the smallest value of the four gaps for that k_y. These new features imply that an Andreev bound state is formed at this energy. However, they are averaged out over k_y and do not stand out in the conductance spectrum. As indicated by the arrows in Fig. 17, at the energies equal to all four values of the gap function at a certain k_y, there appear features in $T(E,k_y)$. It should also be noted that for states with k_y in this region, $T(E,k_y)$ no longer has a counteracting asymmetric $T(E)$ at any other k_y. Therefore, these states contribute to the asymmetry in the conductance spectrum.

Figure 18 depicts example plots of $A(E)$, $B(E)$, and $T(E)$ of the states that consist of four real-k_x excitations and contribute to ZBCP's. For these states, there are in $T(E)$ Lorentzian-like peaks at zero energy as well as features occurring at four energies equal to the four gaps, as indicated by the arrows. For the energy between the smallest and the biggest energy gaps, $T(E,k_y)$ shows the biggest asymmetry and does not have a counteracting asymmetric $T(E)$ at any other k_y. Therefore, these states also contribute to the asymmetry in the tunneling conductance spectrum.

For comparison with the $\nu_S=-0.2$ case, we show the conductance curve for the case of $\nu_S=0.2$ in Fig. 19. The curve is a mirror image of the $\nu_S=-0.2$ case with respect to zero applied voltage. The V-shaped gaplike feature peaks around $\pm 0.52\Delta_{\max}$, which is the magnitude of the gap function at $k_y=\pm\pi$.

For the system with ν_S that provides only two real-k_x transmitted excitations for all k_y, e.g., $\nu_S=-0.6$, $T(E,k_y)$,

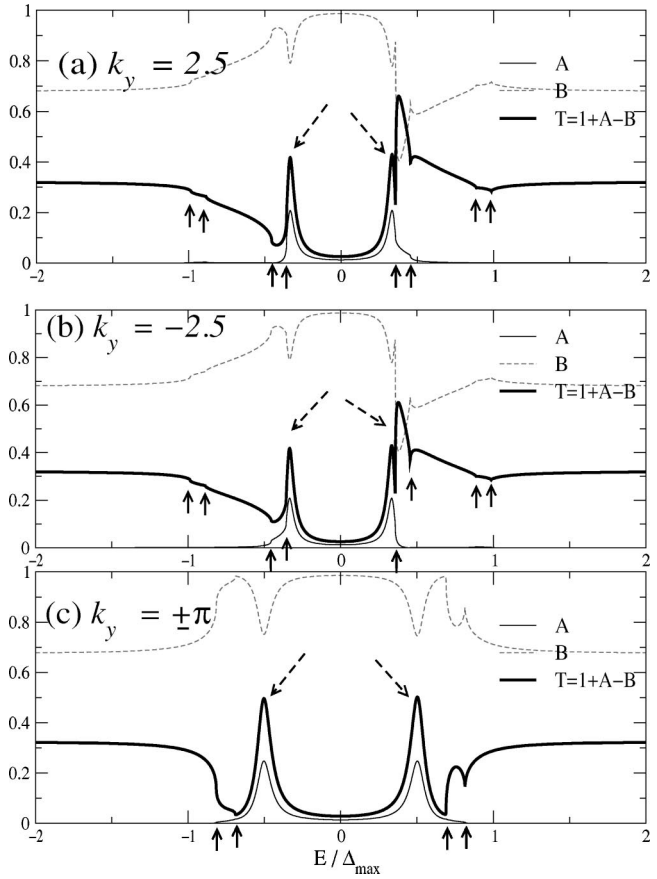

FIG. 17. Plots of $A(E)$, $B(E)$, and $T(E)$ for the states that are not zero-energy bound states in a {210} case for $\nu_S=-0.2$ and the states that contain all four excitations with real k_x. The arrows mark all the values of the gap for each k_y. The dashed arrows indicate the extra features occurring at the energies slightly below the smallest gap.

$A(E,k_y)$, $B(E,k_y)$, and the conductance spectrum have similar characteristics as those in the isotropic model. The conductance spectrum of the $\nu_S=-0.6$ case are displayed in Fig. 20. The V-shaped gaplike feature is not as prominent as in the previous cases. It peaks around $\pm 0.57\Delta_{\max}$, which is the magnitude of the gap function at $k_y=0$.

The tunneling conductance spectra in the {210} case depend on the shape of the Fermi surface. Different band structures produce different ranges of k_y that allow zero-energy surface bound states in a SABZ. For a half-filled band, such bound states do not exist and therefore there is no ZBCP in the tunneling conductance spectrum. Away from a half-filled band the range of k_y that can give zero-energy bound states starts to grow and approaches the corresponding range in the isotropic model. Different Fermi surfaces also cause different ranges of k_y that allow the states, which are made up of four real-k_x excitations. These states are responsible for the asymmetry in the conductance spectrum except for a system of a half-filled band.

As predicted in the isotropic model, the gaplike feature of an NID{210} junction peaks at $\pm 0.60\Delta_{\max}$. In the lattice model, the positions of these peaks are at $\pm\Delta(k_y=0)$ for the systems with less than half-filled bands ($\nu_S<0$) and at

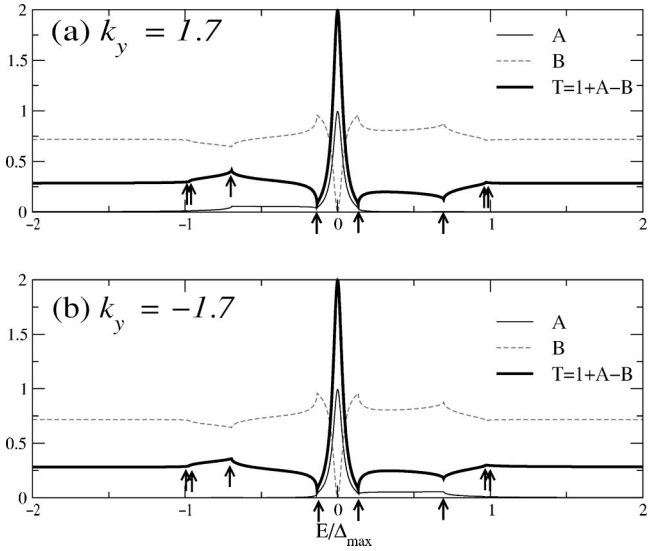

FIG. 18. Plots of $A(E)$, $B(E)$, and $T(E)$ for zero-energy bound states in a {210} case for $\nu_S=-0.2$ and for the states that contain all four excitations with real k_x. The arrows mark all the values of the gap at each k_y.

$\pm\Delta(k_y=\pm\pi)$ for those with more than half-filled bands ($\nu_S>0$). The value of these gaps ranges from (0.50 to 0.60)$\Delta_{\max}$. As the shape of the Fermi surface approaches a circle, i.e., $\nu_S\rightarrow\pm 1$, the peak positions approach the isotropic model prediction (see Fig. 21).

B. Next-nearest-neighbor interactions

In this section we include the next-nearest-neighbor interactions in the calculation, in order to mimic the Fermi surface of YBCO. We consider two cases: {110} and {210}. The {100} case is again similar to that in the isotropic model. In the {110} case for some Fermi surfaces in this approximation, the number of the transmitted excitations is four, the same as in the {210} case in the nearest-neighbor approximation. This can lead to the states of some k_y not contributing to a ZBCP. This fact is not expected in the isotropic model which predicts all states in the {110} case contribute to a ZBCP. As will be discussed below, these nonbound states are composed of four real-k_x excitations and thus cause a small asymmetry in the tunneling conductance. For the {210} case, the dependence of the conductance spectrum on the band structure remains strong upon the addition of next-nearest-neighbor effects. For some bands, the spectra show two extra features that appear at the positions closely related to $\Delta(k_y=0)$ and $\Delta(k_y=\pi)$.

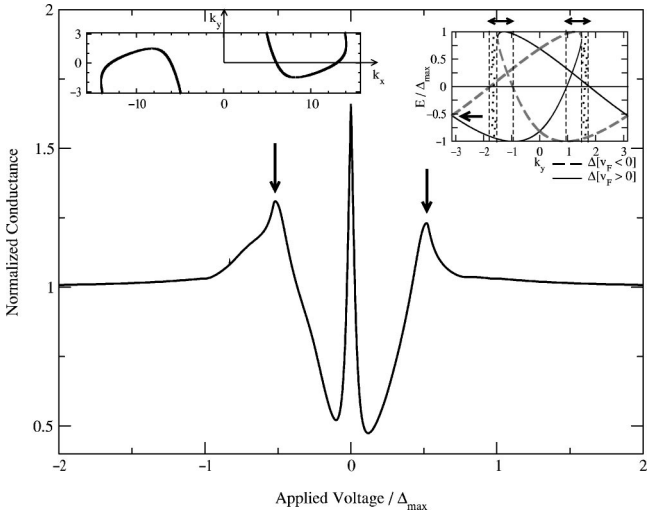

FIG. 19. The conductance spectrum of an NID{210} junction with the superconductor having a $\nu_S=0.2$ Fermi surface (the left inset). The right inset shows the plots of gaps of all propagating excitations as functions of k_y. The regions bounded by the arrows are those where the zero-energy bound states can be formed. The dotted areas are those in which zero-energy bound states are composed of four excitations, only two of which having real k_x. The rest of the areas bounded by the arrows are those in which the bound states are composed of four real-k_x excitations.

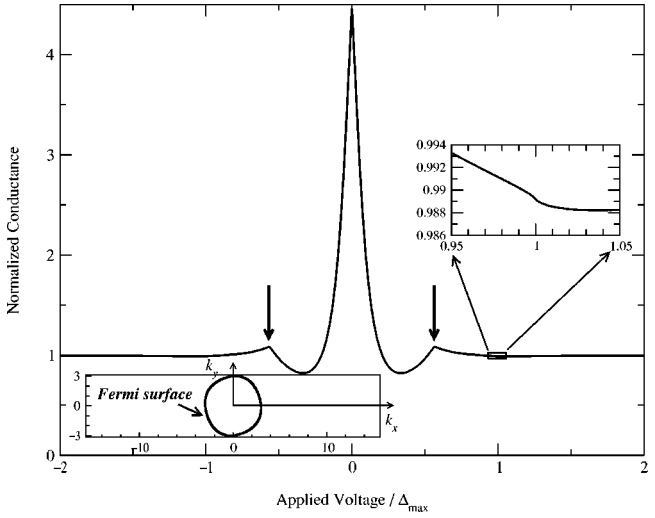

FIG. 20. Tunneling conductance spectrum of an NID{210} junction with the superconductor having a $\nu_S=-0.6$ Fermi surface (the lower left inset). The gaplike feature peaks at $eV=\pm 0.57\Delta_{\max}$. The upper right inset displays an enlargement of the conductance curve around the maximum gap.

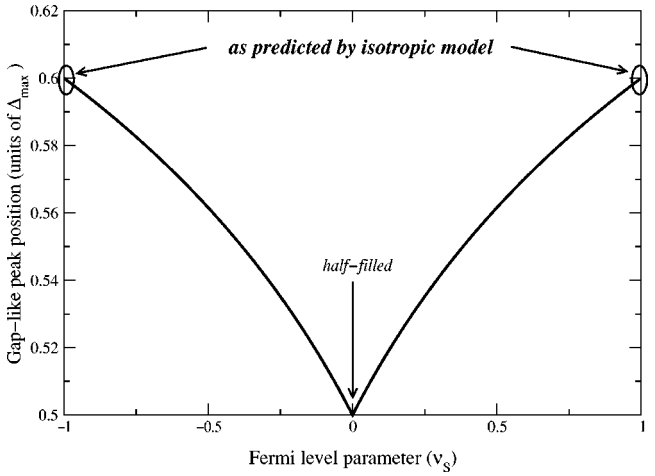

FIG. 21. The plot of the peak position of the gaplike feature occurs in the conductance spectrum of an NID{210} junction as a function of Fermi level.

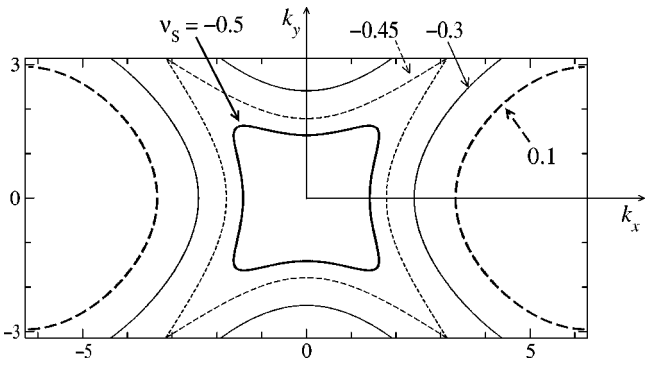

FIG. 22. The SABZ for the {110} case. The contour lines inside the BZ represent Fermi surfaces parametrized by different values of ν_S.

1. The {110} case

The structure of the wave function of the superconductor with the {110} interface in the next-nearest-neighbor approximation is similar to that of the {210} case in the nearest-neighbor case, only with more symmetry. That is, the superconductor wave function is a linear combination of four transmitted excitations as in Eq. (23) but with $k_1=-k_4$ and $k_2=-k_3$ in the case where all $k_j, j=1\cdots4$ are real (also $|\Delta_{k_1}|=|\Delta_{k_4}|$ and $|\Delta_{k_2}|=|\Delta_{k_3}|$), and with $k_1=-k_2$ in the case where only two of k_j are real (also $|\Delta_{k_1}|=|\Delta_{k_2}|$). Four Fermi surfaces in a {110} surface-adapted BZ are plotted in Fig. 22.

As in the {210} case with the nearest-neighbor approximation, for some k_y the states are the superposition of four transmitted excitations, all of which have real k_x, and for other k_y they are the superposition of four excitations, only two of which have real k_x. Only the latter states can satisfy the zero-energy surface bound-state condition. Particularly, for $\nu_S<0$, k_y with $|k_y|<k_y^*\equiv 2\cos^{-1}[(t_S/2t_S')(1-\sqrt{1+4\nu_S t_S'/t_S})]$ can provide zero-energy surface bound states, but k_y out of this range cannot. For $\nu_S>0$, there are no states that are composed of four real-k_x excitations. Thus, all k_y can provide zero-energy surface bound states.

The plots of $A(E)$, $B(E)$, and $T(E)$ at a given k_y, which either do or do not give zero-energy bound states are displayed in Fig. 23. $T(E)$ for the states composed of four real-k_x excitations, which cannot form zero-energy surface bound states, shows a U-shaped gaplike feature which peaks at an energy slightly below the smaller gap [see Figs. 23(c) and 23(d)]. These peaks in $T(E)$ again imply the presence of a resonant Andreev bound state at this energy. These features however do not show up in the conductance spectrum because they are averaged out over k_y. The function $T(E)$ of these states also exhibits asymmetry especially at energies between the two gaps. These states therefore contribute to the asymmetry in the conductance spectrum. The degree of the asymmetry varies with the number of states composed of four real-k_x excitations in the SABZ. The most asymmetric conductance spectrum belongs to the system with $\nu_S=-0.45$ [see Fig. 24(a)]. As depicted in Fig. 24, the main features of the NID{110} conductance are a ZBCP and shoulderlike features at $eV=\pm\Delta_{\max}$.

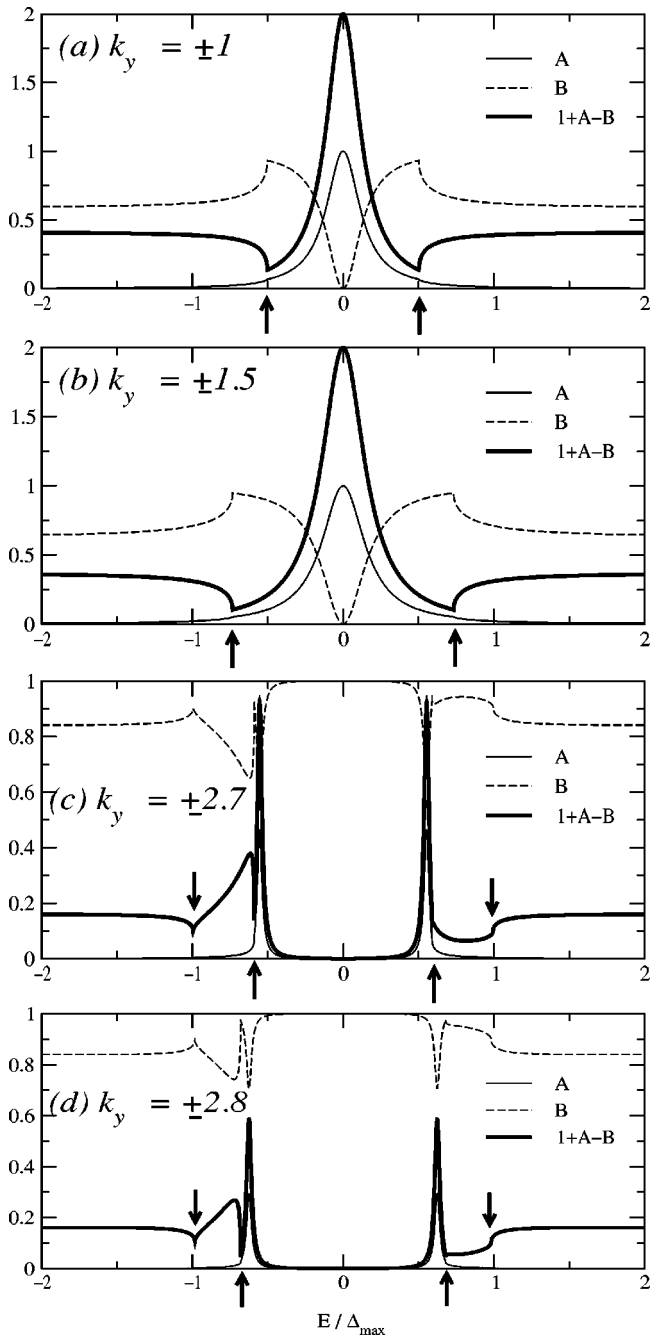

FIG. 23. (a) and (b) show the plots of $A(E)$, $B(E)$, and $T(E)$ of the states that can become zero-energy bound states. (c) and (d) show the plots of the states that cannot be zero-energy bound states. The arrows mark the values of the gap function at a particular k_y. We take $\nu_S=-0.3$.

2. The {210} case

The structure of the wave function that describes the superconductor in this case is a little more complicated than in all the previous cases. It is a linear combination of six transmitted excitations of the same energy and k_y. Figure 25

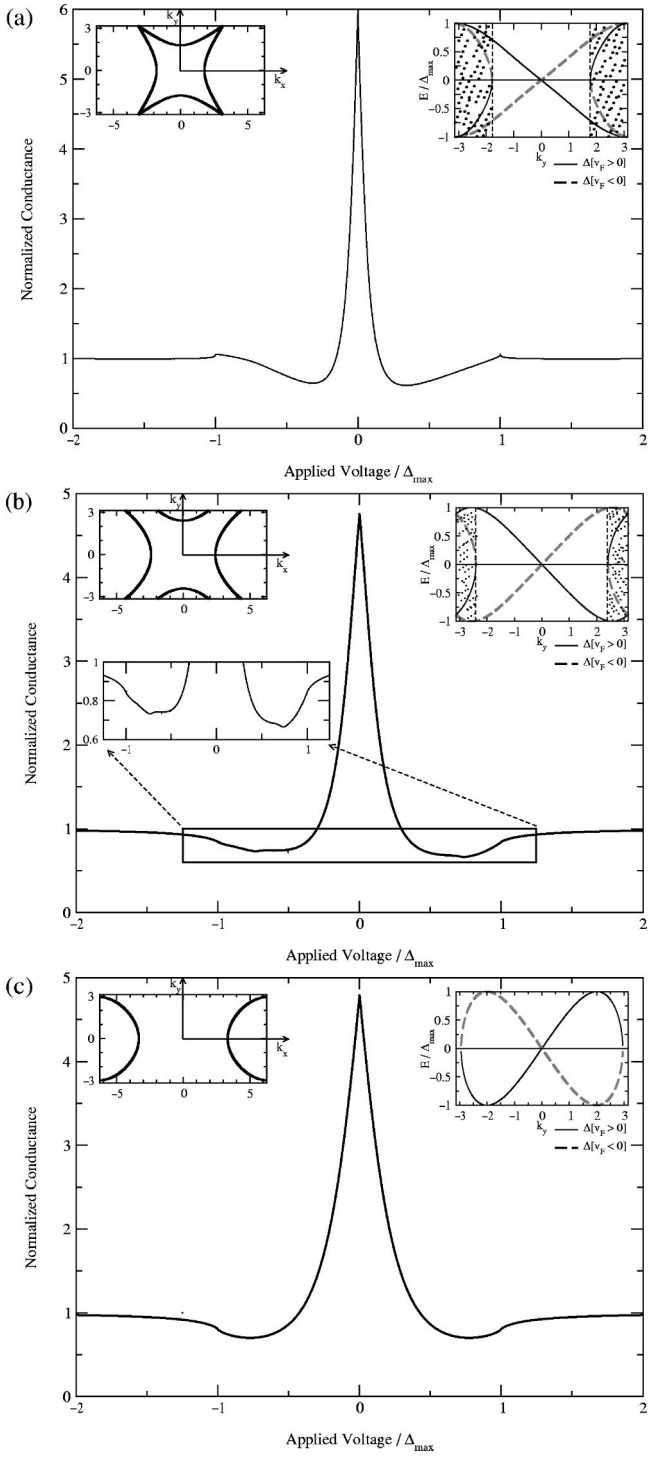

FIG. 24. The normalized conductance spectra of an NID{110} junction for various Fermi surfaces. The upper right inset in each picture shows the plots of all the gaps of propagating excitations. The dotted area in the inset is the region in which the states are not zero-energy surface bound states. The upper left inset shows the Fermi surface plotted in a {110} SABZ. In (b), the lower left inset is an enlarged plot in the boxed region.

shows different Fermi surfaces for the next-nearest-neighbor approximation in a {210} SABZ. The wave function of the superconductor takes the following form:

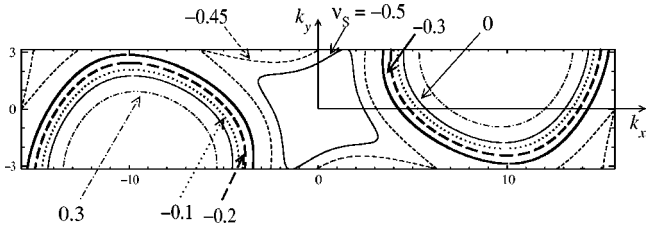

FIG. 25. The SABZ for the {210} case. The contour lines inside the BZ represents Fermi surfaces as parametrized by different ν_S.

$$U_S^{k_y}(n>1)=\sum_{j=1}^{6} c_j \begin{bmatrix} u_{k_{x_j}} \\ v_{k_{x_j}} \end{bmatrix} e^{ik_{x_j} a_S \sqrt{5} n}. \tag{24}$$

Figures 26(a) to 26(d) show the plots of $A(E)$, $B(E)$, and $T(E)$ for different k_y and Fig. 26(e) shows the plots of the gaps of all propagating transmitted excitations as functions of k_y for a system with $\nu_S = -0.3$. For a system with ν_S that provides most states which are composed of six excitations, more than two of which having real k_x, the conductance spectrum shows asymmetry around zero applied voltage. For a system with ν_S that always provides only two excitations with real k_x, its spectrum is symmetric.

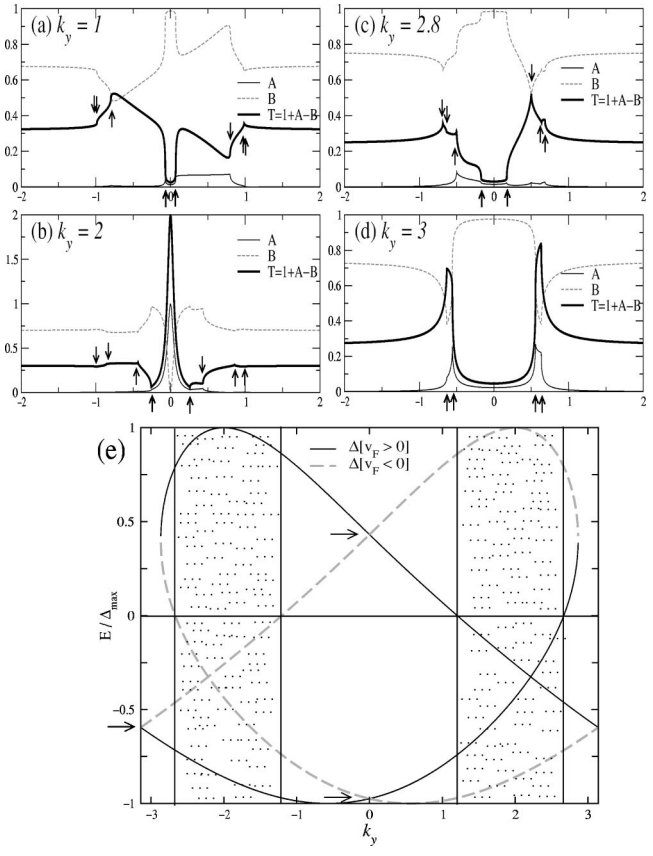

FIG. 26. The plots of $A(E)$, $B(E)$, and $T(E)$ at different k_y for $\nu_S = -0.3$ are in (a)–(d). (e) shows the plot of real energy gaps for all propagating excitations as functions of k_y. The shadowed area indicates the region of k_y that gives $T(E)$, a Lorentzian peak at zero energy.

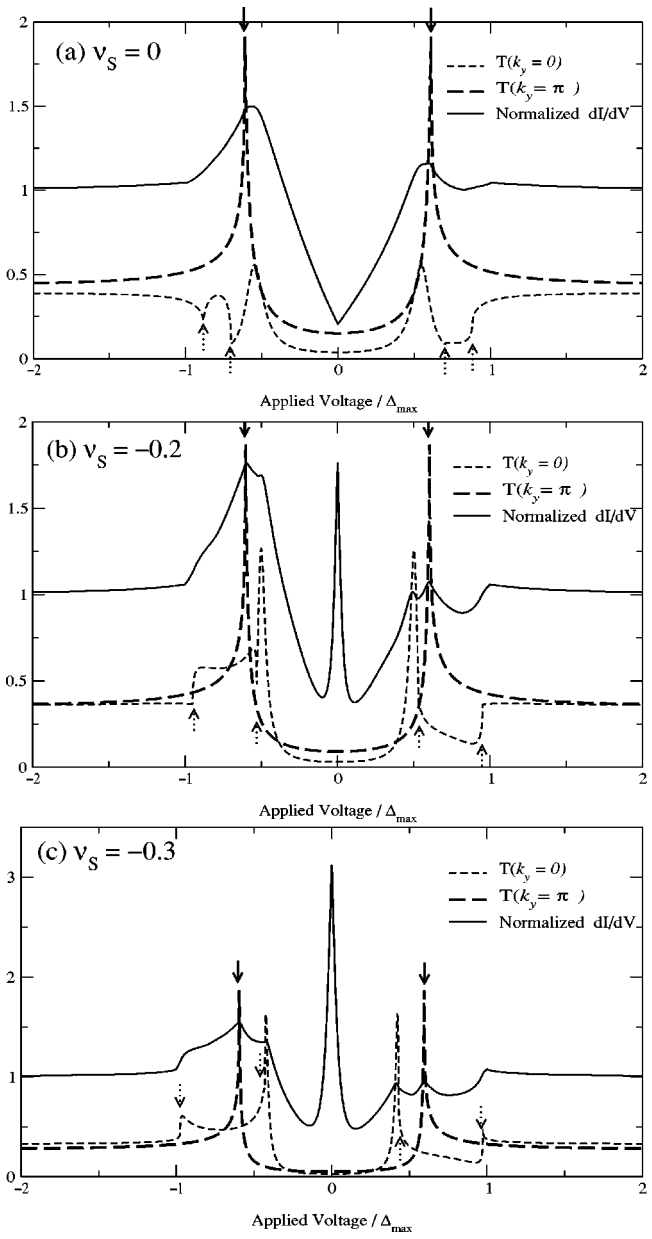

FIG. 27. The plots of the normalized conductance and $T(E,k_y=0,\pi)$ for the systems with ν_S that give asymmetric spectra. The solid arrows indicate $\Delta(k_y=\pi)$ and the dotted arrows indicate $\Delta(k_y=0)$.

Figure 27 shows only a few cases of different ν_S. These cases provide the asymmetric conductance spectra (the solid lines). Similar to the nearest-neighbor case, the conductance spectrum of a system with $\nu_S=0$ does not display a ZBCP. For systems with other ν_S, e.g., -0.2, -0.3, in addition to a ZBCP, there are four cusplike features symmetric in positions. These peaks clearly come from the states with $k_y=0,\pi$ (the thin and thick dashed lines in Fig. 27 respectively).

In summary, for NID{110} junctions with up to next-nearest-neighbor interactions or NID{210} junctions with only nearest interactions, the structures of the wave functions are more complicated than those from the isotropic model due to the elongated SABZ. Their wave functions are linear combinations of more than two excitations. The conductance spectra of these junctions reveal strong dependence on the shape of the Fermi surface. They are asymmetric around zero voltage and contain the cusplike features that occur at voltages other than zero or $\pm\Delta_{max}$. The asymmetry is caused by those states that contain more than two excitations that have real energy gaps (or real k_x) except for the case of a {210} junction with nearest-neighbor interactions and a half-filled band. The cusplike features in fact occur at the voltages equivalent to the energy gaps of the states that have the momenta perpendicular to the surface and of those that have the momenta on the edges of the SABZ.

We should also qualitatively discuss how the self-consistency of the gap function may influence the positions of these cusplike features. As shown in Refs. 28 and 29, for the surface orientation away from {100} the gap function is suppressed over the distance of a few coherence lengths. This suppression is expected to effect the width of the ZBCP and to cause the peaks other than the ZBCP to move a little away from the positions expected when we assume the gap function does not vary spatially.[30] The movement in our case of the cusplike peaks should be approximately of order of the maximum energy gap over the bandwidth of the superconductor times the energy at the position of the peak. This amount of movement would be very small in most cases of high-T_c materials because their bandwidths are at least an order of magnitude larger than the maximum gap.

V. CONCLUSION

Using a 2D discrete lattice model and the BTK formalism, we have studied the differential conductance spectrum of NID junctions. We examined the dependence of the spectrum on both surface orientation and Fermi level of the *d*-wave superconductor. The conductance spectrum are shown to be very sensitive to the Fermi surface for interface orientations away from {100} and {110}. The conductance spectrum shows, in addition to a ZBCP, cusplike peaks that occur at the energy gap of the state with its momentum either perpendicular to the surface, or on the edge of the SABZ. The presence of these cusplike peaks and our ability to predict their positions provide us with an opportunity to use directional tunneling spectroscopy as a tool to map out the magnitude of the energy gap of a *d*-wave superconductor in the momentum space.

ACKNOWLEDGMENTS

We would like to thank the Natural Sciences and Engineering Research Council of Canada for support. P.P. would like to also thank the Royal Thai government for its financial support.

[1] E. L. Wolf, *Principles of Electron Tunneling Spectroscopy* (Oxford University Press, New York, 1985).
[2] W. L. McMillan and J. M. Rowell, in *Superconductivity*, edited by R. D. Parks (Marcel-Dekker, New York, 1969), Vol. 1, p. 561.
[3] I. Giaever, Phys. Rev. Lett. **5**, 147 (1960).
[4] J. Y. T. Wei, N.-C. Yeh, D. F. Garrigus, and M. Strasik, Phys. Rev. Lett. **81**, 2542 (1998).
[5] W. Wang, M. Yamazaki, K. Lee, and I. Iguchi, Phys. Rev. B **60**, 4272 (1999).
[6] I. Iguchi, W. Wang, M. Yamazaki, Y. Tanaka, and S. Kashiwaya, Phys. Rev. B **62**, R6131 (2000).
[7] S. Kashiwaya, Y. Tanaka, M. Koyanagi, and K. Kajimura, Phys. Rev. B **53**, 2667 (1996).
[8] C.-R. Hu, Phys. Rev. Lett. **72**, 1526 (1994).
[9] J. Geerk, X. X. Xi, and G. Linker, Z. Phys. A **73**, 329 (1988).
[10] J. Lesueur, L. H. Greene, W. L. Feldmann, and A. Inam, Physica C **191**, 325 (1992).
[11] S. Kashiwaya, A. Koyanagi, M. Matsuda, M. Matsuda, and K. Kajimura, Physica B **194-195**, 2119 (1994).
[12] M. Covington, R. Scheuerer, K. Bloom, and L. H. Greene, Appl. Phys. Lett. **68**, 1717 (1996); M. Covington, M. Aprili, E. Paraoanu, L. H. Greene, F. Xu, J. Zhu, and C. A. Mirkin, Phys. Rev. Lett. **79**, 277 (1997).
[13] L. Alff, H. Takashima, S. Kashiwaya, N. Terada, H. Ihara, Y. Tanaka, M. Koyanagi, and K. Kajimura, Phys. Rev. B **55**, 14 757 (1997).
[14] J. W. Ekin, Y. Xu, S. Mao, T. Venkatesan, D. W. Face, M. Eddy, and S. A. Wolf, Phys. Rev. B **56**, 13 746 (1997).
[15] J. Y. T. Wei, C. C. Tsuei, P. J. M. van Bentum, Q. Xiong, C. W. Chu, and M. K. Wu, Phys. Rev. B **57**, 3650 (1998).
[16] J. Yang and C. R. Hu, Phys. Rev. B **50**, 16 766 (1994).
[17] G. E. Blonder, M. Tinkham, and T. M. Klapwijk, Phys. Rev. B **25**, 4515 (1982).
[18] J. Demers and A. Griffin, Can. J. Phys. **49**, 285 (1971).
[19] J. Demers and A. Griffin, Phys. Rev. B **4**, 2202 (1971).
[20] Y. Tanaka and S. Kashiwaya, Phys. Rev. Lett. **74**, 3451 (1995).
[21] H. Ding, T. Yokaya, J. C. Campuzano, T. Takahashi, M. Randeria, M. R. Norman, T. Mochiku, K. Kadowaki, and J. Giapintzakis, Nature (London) **382**, 51 (1996); H. Ding, M. R. Norman, J. C. Campuzano, M. Randeria, A. F. Bellman, T. Yokoya, T. Takahashi, T. Mochiku, and K. Kadowaki, Phys. Rev. B **54**, R9678 (1996).
[22] M. C. Schabel, C. H. Park, A. Matsuura, Z. X. Shen, D. A. Bonn, R. Liang, and W. N. Hardy, Phys. Rev. B **55**, 2796 (1997).
[23] M. C. Schabel, C. H. Park, A. Matsuura, Z. X. Shen, D. A. Bonn, X. Liang, and W. N. Hardy, Phys. Rev. B **57**, 6090 (1998).
[24] M. C. Schabel, C. H. Park, A. Matsuura, Z. X. Shen, D. A. Bonn, R. Liang, and W. N. Hardy, Phys. Rev. B **57**, 6107 (1998).
[25] A. F. Andreev, Zh. Éksp. Teor. Fiz. **46** 1823 (1964) [Sov. Phys. JETP **19**, 1228 (1964)].
[26] M. B. Walker and P. Pairor, Phys. Rev. B **59**, 1421 (1999).
[27] Y. Tanuma, Y. Tanaka, M. Yamashiro, and S. Kashiwaya, Phys. Rev. B **57**, 7997 (1998).
[28] Y. Tanuma, Y. Tanaka, M. Ogata, and S. Kashiwaya, Phys. Rev. B **60**, 9817 (1999).
[29] L. J. Buchholtz, M. Palumbo, D. Rainer, and J. A. Sauls, J. Low Temp. Phys. **101**, 1079 (1995).
[30] Yu. S. Barash, A. A. Svidzinsky, and H. Burkhardt, Phys. Rev. B **55**, 15 282 (1997).